Electronic Supplementary Information

Multifunctional metal selenide-based materials synthesized via a one-pot solvothermal approach for electrochemical energy storage and conversion applications

Bhimanaboina Ramulu, Shaik Junied Arbaz, Manchi Nagaraju, and Jae Su Yu*

Department of Electronics and Information Convergence Engineering, Institute for Wearable Convergence Electronics, Kyung Hee University, 1732 Deogyeong-daero, Giheung-gu, Yongin-si, Gyeonggi-do 17104, Republic of Korea

*Corresponding Author. E-mail:jsyu@khu.ac.kr

1. Materials and chemicals

The nickel (Ni) foam and activated carbon (AC) were received from MTI Korea, South Korea. Deionized (DI) water (resistivity: ~ 18.0 MΩ cm) received from a Milli-Q water purification system was used during experiments. Se powder was obtained from Sigma-Aldrich Co., South Korea. Sodium borohydride ($NaBH_4$), iron chloride hexahydrate ($FeCl_3 \cdot 6H_2O$), potassium hydroxide (KOH), polyvinylidene fluoride (PVDF, -$(C_2H_2F_2)_n$-), N-methyl-2-pyrrolidone (NMP, C_5H_9NO), super P carbon black (C65, TIMCAL), hydrochloric acid (HCl), ethylene glycol (EG), and absolute ethanol were purchased from Daejung Chemicals Ltd., South Korea. All of the compounds were of analytical quality and were utilized just as they were received, with no additional purification.

2. Characterizations

The morphological and elemental mapping images of the prepared materials were studied by using a field-emission scanning electron microscope (FE-SEM, Carl Zeiss, LEO SUPRA 55, 5 kV) equipped with the energy-dispersive X-ray (EDX) spectroscopy analysis. X-ray diffraction (XRD, M18XHF-SRA, Mac Science) analysis was performed. The surface chemical composition and oxidation states of the elements in the material were evaluated by X-ray photoelectron spectroscopy (XPS, Thermo Electron MultiLab2000).

3. Electrochemical measurements

All the electrochemical properties were measured by using an Iviumstat electrochemical workstation (The Netherlands). The electrochemical performance was measured using a beaker-type three-electrode cell consisting of Ni foam (active area of 1 × 1 cm^2) comprising electroactive materials, Ag/AgCl, and platinum (Pt) wire as the working, reference, and counter electrodes,

respectively, in aqueous 2 M KOH electrolyte. The electrochemical measurements including cyclic voltammetry (CV), galvanostatic charge-discharge (GCD), and electrochemical impedance spectroscopy (EIS, frequency range: 0.01 Hz to 100 kHz with 5 mV amplitude) studies were performed at room temperature. The AC-coated Ni foam (AC/Ni foam) was prepared by grinding AC with super P carbon black and PVDF as the binder dissolved in NMP solvent in a weight ratio of 80:10:10. The resulting slurry was brush-coated onto the Ni foam (with the active area of 1×1 cm^2) with a mass loading of ~ 1.5 mg cm^{-2} and dried at 100 °C for 3 h in a vacuum oven. The areal capacity and specific capacitance of the prepared materials were estimated using the following formulae:[1-3]

$$C_A = \frac{2I \int v(t)\, dt}{a \times V} \quad \text{(S1)}$$

$$C_s = \frac{I \times \Delta t}{m \times \Delta V} \quad \text{(S2)}$$

where 'C_A' and 'C_s' are the areal capacity (Ah cm^{-2}) and specific capacitance (F g^{-1}), respectively. '$\int v(t)dt$' is an integral area (V s) of the discharge curve, 'I' is the applied current (A), 'a' is the active area of the electrode (cm^2), 'ΔV' is the potential window (V), 'm' is the mass of the electrode (g), and 'Δt' is the discharge time (s).

4. Construction of pouch-type aqueous hybrid cell (AHC)

For a two-electrode design, a pouch-type AHC was constructed using a battery-type FeNiSe-15 h/Ni foam as the positive electrode and capacitive-like AC/Ni foam as the negative electrode in 2 M KOH electrolyte. In the device construction, a slice of filter paper was placed in between the electrodes to prevent a short-circuit. Later, the complete sandwich assembly was carefully closed

with a pouch-type parafilm bag using a commercial-grade heat sealer. To balance the charges on both electrodes, the mass balancing of the positive electrode to the negative electrode (AC) was estimated using the following formula:[4,5]

$$m_{-} = \frac{Q_{+} \times a_{+}}{C_{-} \times \Delta V_{-}} \quad \text{(S3)}$$

where Q_+ and a_+ represent the areal capacity (Ah cm^{-2}) and active area (cm^2) of the positive electrode, and m_- is the mass (g), C_- is the specific/areal capacitance (F g^{-1}/F cm^{-2}), and ΔV_- is the potential window (V) of the negative electrode, respectively.

The areal energy density and power density of the assembled AHC device were calculated using the below formulas:[6,7]

$$E = \frac{I \times \int v(t)\, dt}{a} \quad \text{(S4)}$$

$$P = \frac{E}{\Delta t} \quad \text{(S5)}$$

where 'I' is the applied current (A), 'a' is the active area of the electrode (cm^2), '$\int v(t)\, dt$' is an integral area (V s) of the discharge curve, and 'E' is the areal energy density (Wh cm^{-2}) and 'P' is the areal power density (W cm^{-2}), respectively.

5. Strategy for self-charging wind turbine//AHC unit

In the strategy for a self-charging unit, two pouch-like AHCs were connected in a series, which are further connected to a commercially obtained wind turbine via connecting wires, as presented in Fig. S7. The wind turbine was driven using continuous airflow, which is connected to the DC

power supply. Before charging the devices, to get desired voltage (3.2 V) for two AHCs, the voltage was controlled by varying the airflow to the wind turbine, as shown in Fig. S7. Once the certain speed of the wind turbine was optimized, we charged the AHCs for further use.

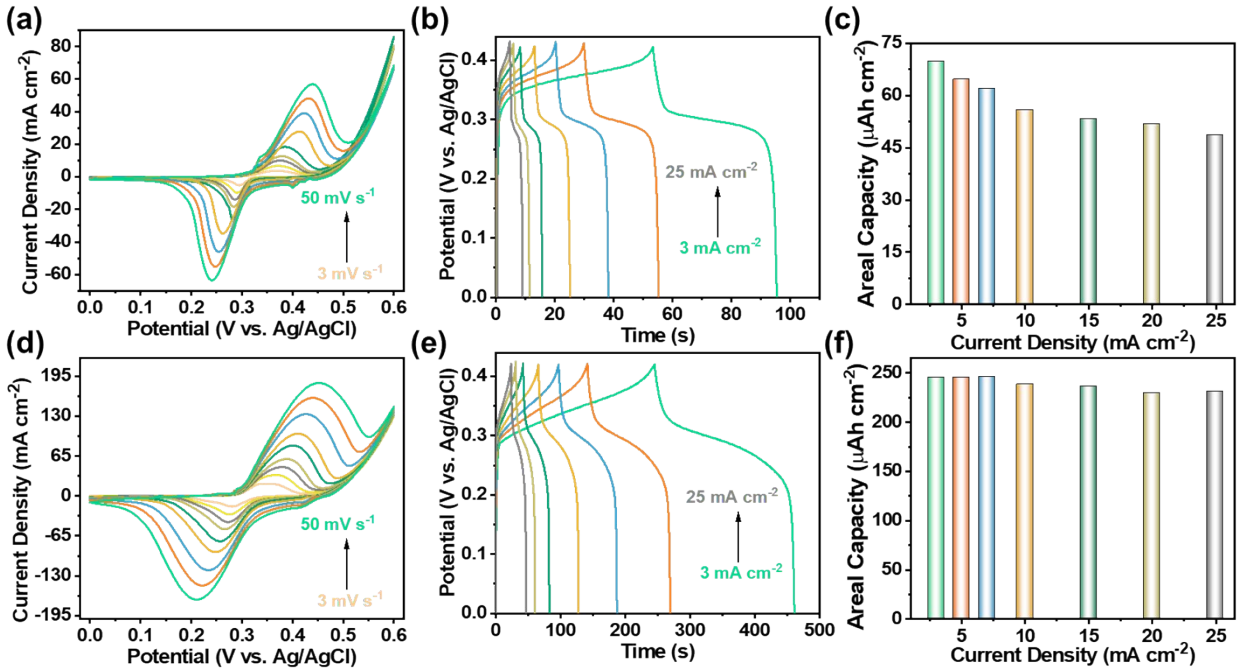

Figure S1. (a) CV curves, (b) GCD curves, and (c) areal capacity values of the FeNiSe-12 h. (d) CV curves, (e) GCD curves, and (f) areal capacity values of the FeNiSe-18 h.

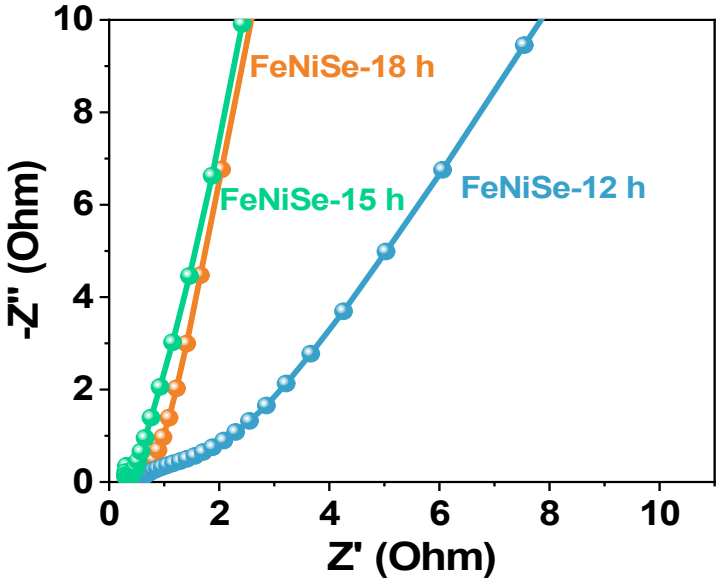

Figure S2. EIS plots of the prepared FeNiSe-12 h, FeNiSe-15 h, and FeNiSe-18 h catalysts.

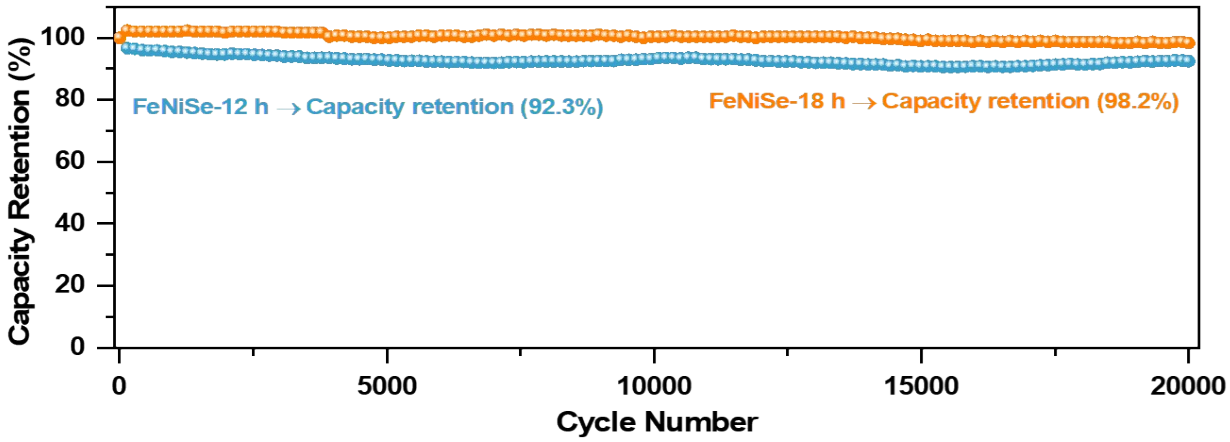

Figure S3. Long-term cycling performance of the FeNiSe-12 h and FeNiSe-18 h electrodes.

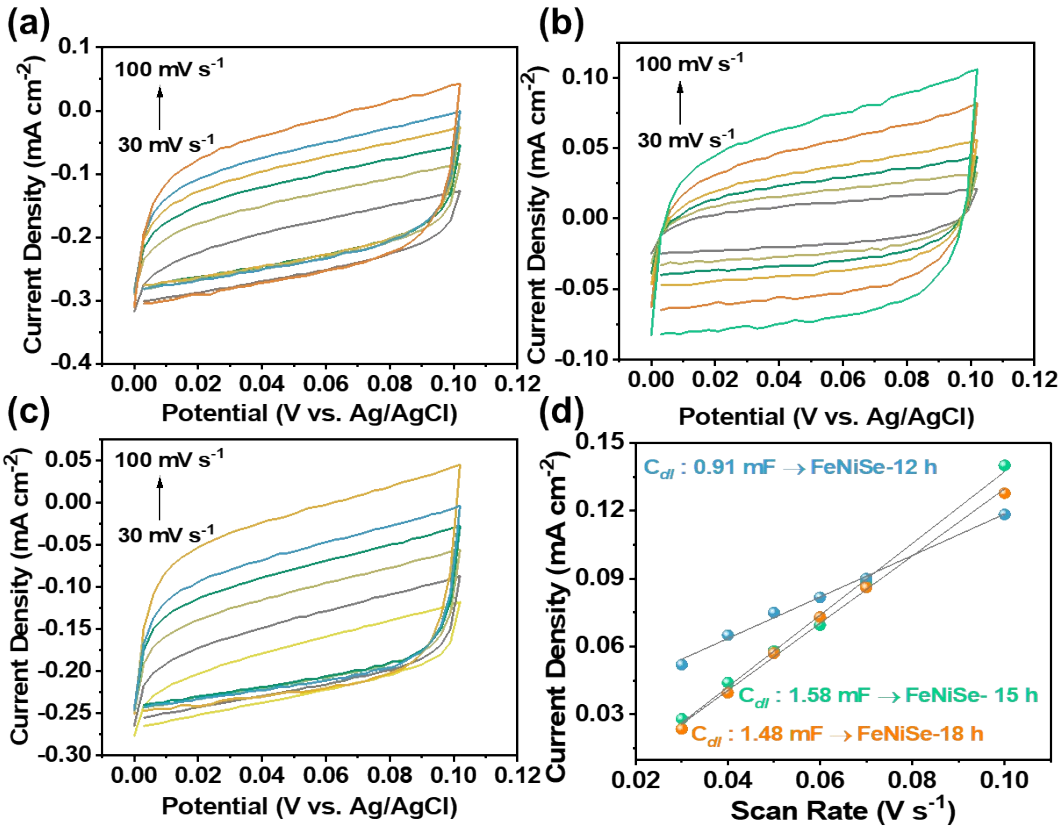

Figure S4. CV curves of the (a) FeNiSe-12 h, (b) FeNiSe-15 h, and (c) FeNiSe-18 h catalysts recorded in 2 M KOH for the ECSA measurement. (d) Plots of scan rate vs. current density obtained from CV data.

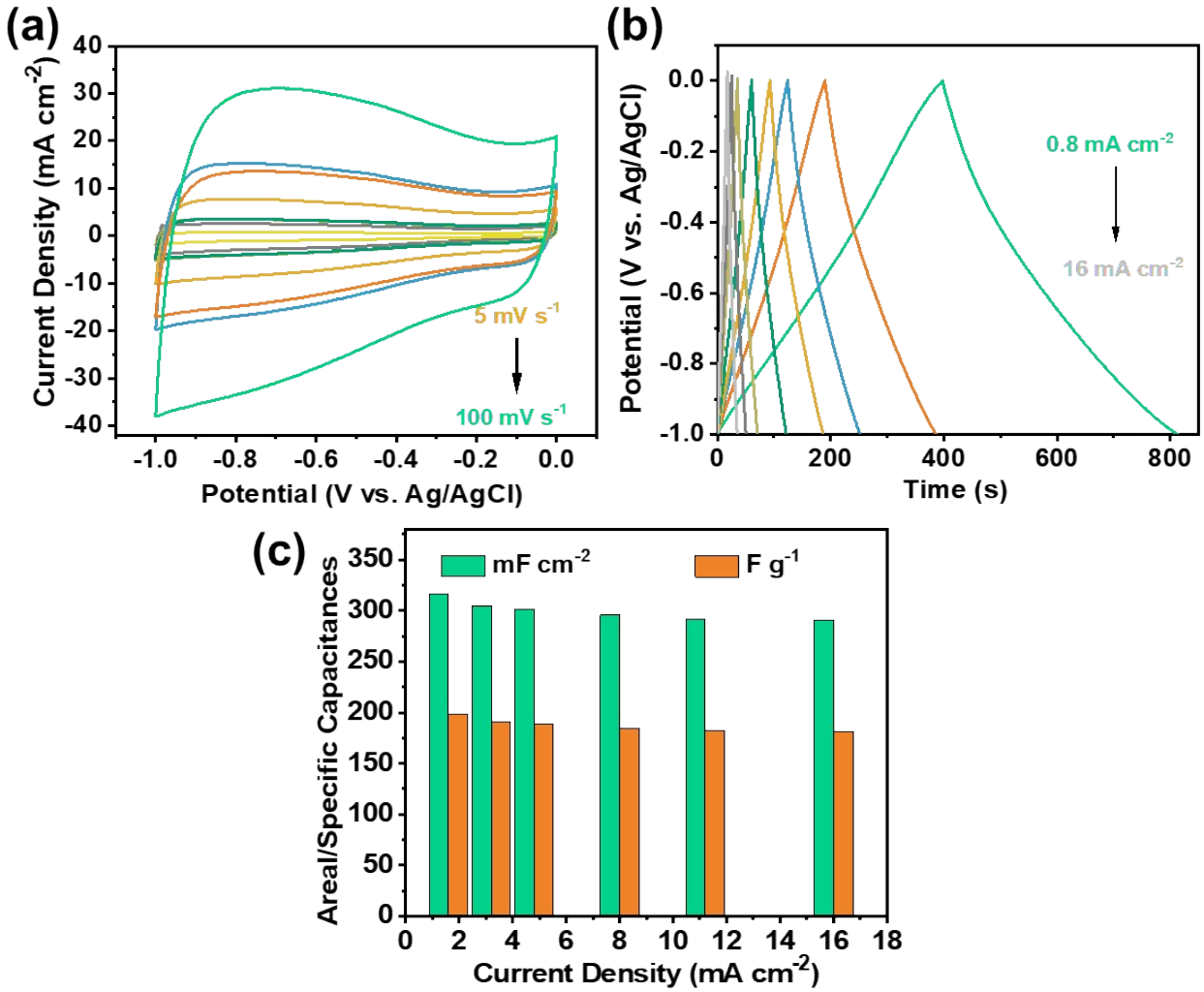

Figure S5. (a) CV curves, (b) GCD curves, and (c) areal/specific capacitance values of the AC-coated Ni foam.

Table S1. Comparative charge storage performance of the $Fe_3Se_4/Ni_{0.85}Se$//AC HC device with the previously reported metal selenide-based devices.

Positive material	Negative material	Applied voltage/electrolyte	Test condition	Energy density	Ref.
$Co_{0.85}Se$	N-PCNs	1.6 V/2 M KOH	0.5 A g^{-1}	21.1 Wh kg^{-1}	S8
$Ni_{0.9}Co_{1.92}Se_4$	AC	1.5 V/3 M KOH	2 mA cm^{-2}	26.2 Wh kg^{-1}	S9
H-$NiCoSe_2$	AC	1.5 V/6 M KOH	0.25 A g^{-1}	25.5 Wh kg^{-1}	S10
$(Ni_{0.1}Co_{0.9})_9Se_8$	rGO	1.55 V/1 M KOH	0.2 A g^{-1}	17 Wh kg^{-1}	S11
$Ni@Ni_{0.8}Co_{0.2}Se$	AC	1.45 V/2 M KOH	1 A g^{-1}	17 Wh kg^{-1}	S12
Ni_3Se_2	AC	1.6 V/2 M KOH	0.2 A g^{-1}	22.3 Wh kg^{-1}	S13
$NiSe_2$@CNT	AC	1.6 V/6 M KOH	1 A g^{-1}	25.6 Wh kg^{-1}	S14
CoSe	AC	1.5 V/2 M KOH	2 A g^{-1}	18.6 Wh kg^{-1}	S15
$CoSe_2$	AC	1.6 V/6 M KOH	0.5 A g^{-1}	18.9 Wh kg-1	S16
$NiCo_2Se_4$	AC	1.6V/6 M KOH	0.5 A g^{-1}	25.0 Wh kg^{-1}	S17
$Ni_{0.85}Se$|P	AC	1.6 V/1 M KOH	1 A g^{-1}	20.7 Wh kg^{-1}	S18
NiSe-Se	AC	1.6 V/1 M KOH	4 mA cm^{-2}	29.9 W h kg^{-1}	S19
$Fe_3Se_4/Ni_{0.85}Se$	**AC**	**1.6 V/2 M KOH**	**3 mA cm^{-2}**	**0.36 mWh cm^{-2} 30.4 Wh kg^{-1}**	**This work**

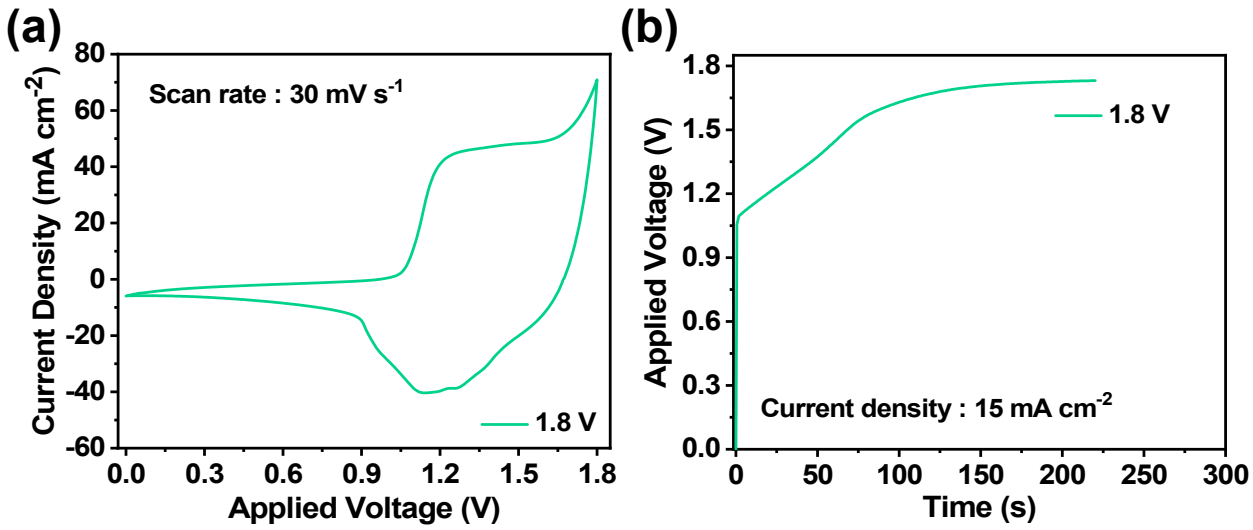

Figure S6. (a) CV curve and (b) GCD curve of the AHC device measured at 1.8 V.

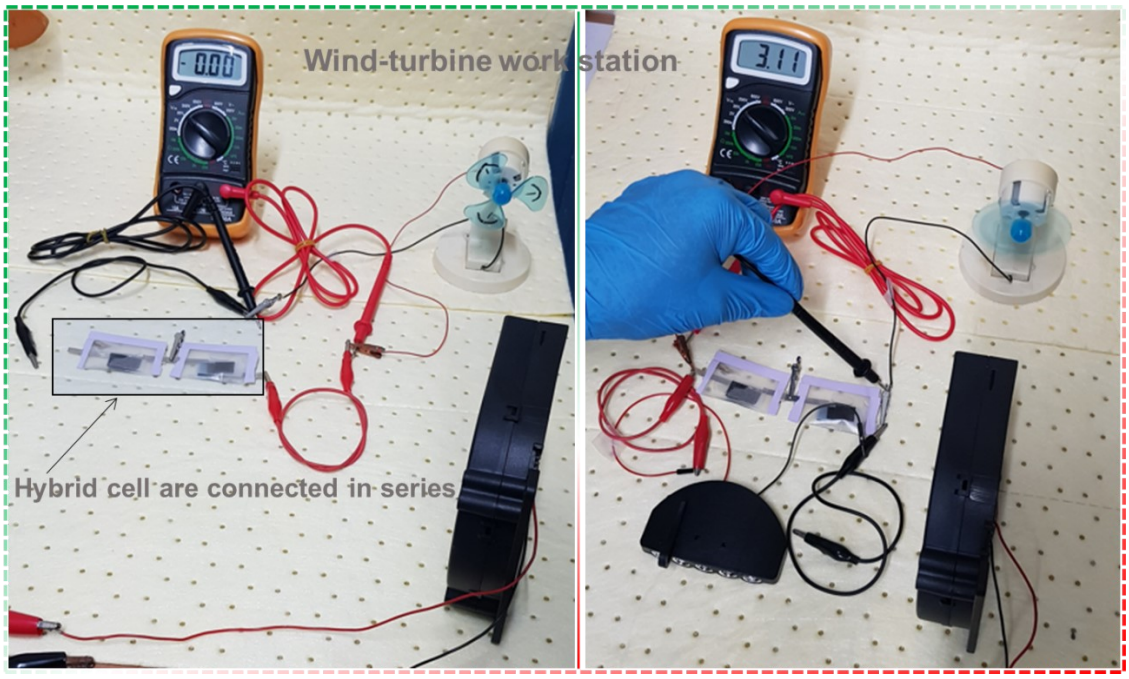

Figure S7. Wind turbine workstation for charging the constructed AHCs.

References

[S1] C. J. Raj, R. Manikandan, P. Thondaiman, P. Sivakumar, A. D. Savariraj, W.-J. Cho, B. C. Kim and H. Jung, *Carbon,* 2021, **184**, 266-276.

[S2] M. Ramu, J. R. Chellan, N. Goli, P. Joaquim, V. Cristobal and B. C. Kim, *Adv. Funct. Mater.,* 2020, **30**, 1906586.

[S3] G. Nagaraju, S. C. Sekhar, B. Ramulu, L. K. Bharat, G. S. R. Raju, Y.-K. Han and J. S. Yu, *Nano Energy*, 2018, **50**, 448-461.

[S4] S. J. Arbaz, S. C. Sekhar, G. Nagaraju, B. Ramulu and J. S. Yu, *Adv. Mater. Technol.,* 2021, **6**, 2000793.

[S5] S. C. Sekhar, B. Ramulu, S. J. Arbaz, S. H. Jin, H. S. Oh and J. S. Yu, *Small Methods,* 2021, **5**, 2100907.

[S6] G. S. Rama Raju, E. Pavitra, G. Nagaraju, N. R. Chodankar, S. K. Vishwanath, J. Y. Park, Y. S. Huh and Y.-K. Han, *J. Mater. Chem. A*, 2019, **7**, 26893-26904.

[S7] A. R. Mule, B. Ramulu and J. S. Yu, *Electrochim. Acta,* 2022, **401**, 139499.

[S8] H. Peng, G. Ma, K. Sun, Z. Zhang, J. Li, X. Zhou and Z. Lei, *J. Power Sources,* 2015, **297**, 351-358.

[S9] W. An, L. Liu, Y. Gao, Y. Liu and J. Liu, *RSC Adv.,* 2016, **6**, 75251-75257.

[S10] L. Hou, Y. Shi, C. Wu, Y. Zhang, Y. Ma, X. Sun, J. Sun, X. Zhang and C. Yuan, *Adv. Funct. Mater.,* 2018, **28**, 1705921.

[S11] P. Yang, Z. Wu, Y. Jiang, Z. Pan, W. Tian, L. Jiang and L. Hu, *Adv. Energy Mater.,* 2018, **8**, 1801392.

[S12] K. Guo, S. Cui, H. Hou, W. Chen and L. Mi, *Dalton Trans.,* 2016, **45**, 19458-19465.

[S13] L. Zhao, P. Zhang, Y. Zhang, Z. Zhang, L. Yang and Z.-G. Chen, *J Mater Sci Technol.,* 2020, **54**, 69-76.

[S14] Y. Zheng, Y. Tian, S. Sarwar, J. Luo and X. Zhang, *J. Power Sources,* 2020, **452**, 227793.

[S15] Y. Zhu, Z. Huang, Z. Hu, L. Xi, X. Ji and Y. Liu, *Electrochim. Acta,* 2018, **269**, 30-37.

[S16] S. Liu, S. Sarwar, J. Wang, H. Zhang, T. Li, J. Luo and X. Zhang, *J. Mater. Chem. C*, 2021, **9**, 228-237.

[S17] S. Li, Y. Ruan and Q. Xie, *Electrochim. Acta,* 2020, **356**, 136837.

[S18] Y. Zhang, T. Wang, Y. Wang, Y. Wang, L. Wu, Y. Sun, X. Zhou, W. Hou, Y. Du and W. Zhong, *Electrochim. Acta,* 2019, **303**, 94-104.

[S19] S. Subhadarshini, E. Pavitra, G. S. Rama Raju, N. R. Chodankar, D. K. Goswami, Y.-K. Han, Y. S. Huh and N. C. Das, *ACS Appl. Mater. Interfaces,* 2020, **12**, 29302-29315.